show a characteristic 'U' shape (Fig. 5a). This gives rise to a remarkable chaotic travelling-wave structure which may be seen in the eight lattice 'snapshots' of Fig. 5b–i. Population abundances in the meta-community remain chaotic, but periodic circular waves continuously expand and contract radially as they spread in time across the spatial landscape. Field and model population studies of the Canadian hare–lynx cycle and European vole cycles have found similar travelling-wave structures with spatially distributed U-shaped phase lags[10,25–27]. Different types of realistic diffusion barrier were introduced into the model but, in general, they failed to destroy the spatial circular wave structure (B.B. *et al.*, manuscript in preparation).

The spatio-temporal structures associated with phase synchronization have important implications for conservation ecology. Even if a disturbance perturbs a local patch population to the brink of extinction, the periodicity of spatial phase syncrhonization guarantees the recurring arrival of wave fronts in which new colonizers will buffer the endangered population. In contrast to the common view of population synchronization as a cause of global population extinctions[14], it appears that phase synchronization can be important for maintaining species persistence. Our findings indicate that synchronization is a powerful process that has the potential to shape the distribution and abundance of species over all scales, from local to continental. We expect that the complex synchronization phenomena identified here will provide new insight into the dynamics of spatial ecologies and will have important applications to the study of biological rhythms in general. □

Received 22 January; accepted 29 March 1999.

1. Elton, C. & Nicholson, M. The ten-year cycle in numbers of the lynx in Canada. *J. Anim. Ecol.* **11,** 215–244 (1942).
2. May, R. M. *Stability and Complexity in Model Ecosystems* (Princeton University Press, Princeton, 1973).
3. Keith, L. B. *Wildlife's 10-year cycle* (University of Wisconsin Press, Madison, 1963).
4. Hanski, I., Turchin, P., Korpimaki, E. & Henttonen, H. Population oscillations of boreal rodents: regulation by mustelid predators leads to chaos. *Nature* **364,** 232–235 (1993).
5. Sinclair, A. R. E. *et al.* Can the solar cycle and climate synchronize the snowshoe hare cycle in Canada? Evidence from tree rings and ice cores. *Am. Nat.* **141,** 173–198 (1993).
6. Royama, T. *Analytical Population Dynamics* (Chapman & Hall, London, 1992).
7. Moran, P. A. P. The statistical analysis of the Canadian lynx cycle. *Aust. J. Zool.* **1,** 291–298 (1953).
8. Bulmer, M. G. A statistical analysis of the 10-year cycle in Canada. *J. Anim. Ecol.* **43,** 701–718 (1974).
9. Korpimaki, E. & Krebs, C. J. Predation and population cycles of small mammals. A reassessment of the predation hypothesis. *BioScience* **46,** 754–764 (1996).
10. Ranta, E., Kaitala, V. & Lundberg, P. The spatial dimension in population fluctuations. *Science* **278,** 1621–1623 (1997).
11. Schaffer, W. Stretching and folding in lynx fur returns: Evidence for a strange attractor in nature? *Am. Nat.* **124,** 798–820 (1984).
12. Rosenblum, M. G., Pikovsky, A. S. & Kurths, J. Phase synchronization of chaotic oscillators. *Phys. Rev. Lett.* **76,** 1804–1807 (1996).
13. Schafer, C., Rosenblum, M. G., Kurths, J. & Abel, H. Heartbeat synchronized with ventilation. *Nature* **392,** 239–240 (1998).
14. Earn, D. J. D., Rohani, P. & Grenfell, B. Persistence, chaos and synchrony in ecology and epidemiology. *Proc. R. Soc. Lond. B* **265,** 7–10 (1998).
15. May, R. M. Simple mathematical models with very complicated dynamics. *Nature* **261,** 459–467 (1976).
16. Stone, L. Period-doubling reversals and chaos in simple ecological models. *Nature* **365,** 617–620 (1993).
17. Blasius, B., Neff, R., Beck, F. & Lüttge, U. Oscillatory model of Crassulacean acid metabolism with a dynamic hysteresis switch. *Proc. R. Soc. Lond. B* **266,** 93–101 (1999).
18. Gurney, W. S. C., Crowley, P. H. & Nisbet, R. M. Locking life-cycles on to seasons: circle-map models of population dynamics and local adaptation. *J. Math. Biol.* **30,** 251–279 (1992).
19. Hastings, A. & Powell, T. Chaos in a three-species food chain. *Ecology* **72,** 896–903 (1991).
20. Gilpin, M. E. Spiral chaos in a predator–prey model. *Am. Nat.* **107,** 306–308 (1979).
21. Vandermeer, J. Seasonal isochronic forcing of Lotka Volterra equations. *Progr. Theor. Phys.* **71,** 13–28 (1996).
22. Gotelli, N. J. *A Primer of Ecology* (Sinauer, Massachusetts, 1995).
23. Pecora, L. M. & Carroll, T. L. Synchronization in chaotic systems. *Phys. Rev. Lett.* **64,** 821 (1990).
24. Cohen, A. H., Holmes, P. J. & Rand, R. H. The nature of the coupling between segmental oscillators of the lamprey spinal generator for locomotion: a mathematical model. *J. Math. Biol.* **13,** 345–369 (1982).
25. Ranta, E. *et al.* Solar activity and hare dynamics: A cross-continental comparison. *Am. Nat.* **149,** 765–775 (1997).
26. Sinclair, A. R. E. & Gosline, M. Solar activity and mammal cycles in the northern hemisphere. *Am. Nat.* **149,** 776–784 (1997).
27. Ranta, E. & Kaitala, V. Travelling waves in vole population dynamics. *Nature* **390,** 456 (1997).
28. Stenseth, N. C., Falck, W., Bjornstad, O. N. & Krebs, C. J. Population regulation in snowshoe hare and Canadian lynx: Asymmetric food web configurations between hare and lynx. *Proc. Natl Acad. Sci. USA* **94,** 5147–5152 (1997).
29. O'Donoghue, M. *et al.* Functional response of coyotes and lynx to the snowshoe hare cycle. *Ecology* **79,** 1193–1208 (1998).
30. Wolf, J. B., Swift, H. L. & Vastano, J. A. Determining Lyapunov exponents from a time series. *Physica D* **16,** 285–317 (1982).

Supplementary information is available on *Nature*'s World-Wide Web site (http://www.nature.com) or as paper copy from the London editorial office of *Nature*.

Acknowledgements. We thank MINERVA for their award of a Fellowship to B.B., and H. Bhasin for her comments on the manuscript.

Correspondence and requests for materials should be addressed to L.S. (e-mail: lewi@lanina.tau.ac.il).

Auditory collusion and a coupled couple of outer hair cells

Hong-Bo Zhao & J. Santos-Sacchi

Sections of Otolaryngology and Neurobiology, Yale University School of Medicine, 333 Cedar Street, New Haven, Connecticut 06510, USA

The discrepancies between measured frequency responses of the basilar membrane in the inner ear and the frequency tuning found in psychophysical experiments led to Békésy's idea of lateral inhibition in the auditory nervous system[1]. We now know that basilar membrane tuning can account for neural tuning[2], and that sharpening of the passive travelling wave depends on the mechanical activity of outer hair cells (OHCs)[3], but the mechanism by which OHCs enhance tuning remains unclear. OHCs generate voltage-dependent length changes at acoustic rates[4–8], which deform the cochlear partition[9–11]. Here we use an electrical correlate of OHC mechanical activity, the motility-related gating current, to investigate mechano-electrical interactions among adjacent OHCs. We show that the motility caused by voltage stimulation of one cell in a group evokes gating currents in adjacent OHCs. The resulting polarization in adjacent cells is opposite to that within the stimulated cell, which may be indicative of lateral inhibition. Also such interactions promote distortion and suppression in the electrical and, consequently, the mechanical activity of OHCs. Lateral interactions may provide a basis for enhanced frequency selectivity in the basilar membrane of mammals.

The mechanical response of the OHC is mirrored by an electrical signature, a motility-related charge movement, similar to the gating charge movements that control ion-channel conductance[12,13]. Both gating currents arise from a redistribution of charged voltage sensors across the membrane. The magnitude of the gating current reflects the rate of charge redistribution. In the OHC, the redistribution of motility-related charge is controlled by both voltage and membrane tension; consequently, either can evoke gating currents[14–16]. Within the organ of Corti, OHCs are indirectly mechanically coupled to each other through contacts with supporting Deiters' cells. The apical regions of OHCs and Deiters' cells are joined by tight junctions and form the plate-like reticular lamina. Basally, the OHCs sit in the cups of Deiters' cells, and the strength of these attachments varies along the length of the basilar membrane[17]. This morphology makes it likely that the voltage-induced mechanical responses of one OHC will affect surrounding OHCs. Determining the nature of this interaction may provide insight into the process of fine frequency tuning by OHCs. We studied this interaction by simultaneously recording from adjacent OHCs under dual whole-cell voltage and current clamp.

In isolated pieces of Corti's organ, where cellular relations remain intact, voltage stimulation of an OHC induces mechanical responses and gating currents in that cell (Fig. 1). Transient outward currents are generated by the onset of depolarization, which causes the cell to contract (Fig. 1b). These currents correspond to the displacement of positive charge to the extracellular aspect of the lateral plasma membrane, which holds motility/voltage sensors[18,19]. The charge–voltage (Q–V) function is well described by a two-state

© 1999 Macmillan Magazines Ltd

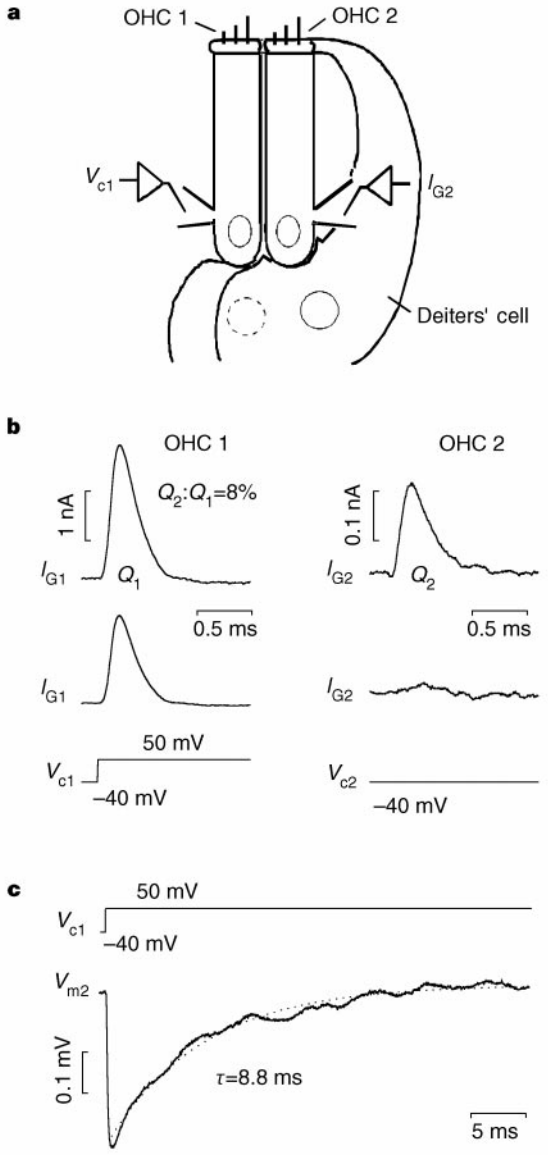

Figure 1 Adjacent OHCs are mechano-electrically coupled. **a**, Schematic illustrating two adjacent OHCs mechanically coupled through Deiters' cells and the recording configuration. **b**, Each cell in a pair was whole-cell voltage clamped to –40 mV. Depolarization of OHC 1 to 50 mV (V_{c1}) generates outward transient currents in both OHC 1 and OHC 2 (I_{G1}, I_{G2}, respectively; top two traces). The charge ratio (Q_2/Q_1) is 0.08. Following application of negative pressure (~–0.5 kPa; middle two traces) to the patch pipette of OHC 1, the response in OHC 2 was abolished. The response in the voltage-stimulated cell is decreased somewhat, as expected, owing to a negative shift in its Q–V function[16]. **c**, OHC 1 was held under voltage clamp and OHC 2 under current clamp. As a consequence of the impulsive gating current evoked in OHC 2, a negative voltage is developed across its membrane. The trace depicts the average induced potential ($n = 7$) in OHC 2. Dotted line: single exponential fit of 8.8 ms.

Boltzmann function[12,13]:

$$Q(V) = \frac{Q_{max}}{1+b} \quad (1)$$

$$b = \exp\left(\frac{-ze(V_m - V_b)}{kT}\right)$$

where Q_{max} is the maximum nonlinear charge moved, V_h is the voltage at half-maximal gating-charge transfer, V_m is the membrane potential, z is the valence, e is the electron charge, k is Boltzmann's constant and T is the absolute temperature.

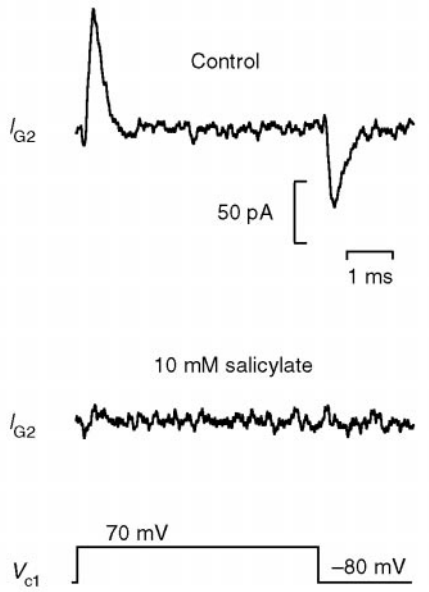

Figure 2 Both OHCs were voltage clamped to –80 mV, and OHC 1 was stepped to 70 mV (V_{c1}). The top trace shows the gating current (I_{G2}) evoked in OHC 2. Perfusion of the cells with 10 mM salicylate abolishes the gating current.

When the stimulated OHC (OHC 1) is depolarized, gating currents are seen in the adjacent OHC (OHC 2). The ratio of charge movement (Q_2/Q_1) in adjacent OHCs can be up to 0.1. The induced gating current in OHC 2 is not generated by electrical interactions between the cells. Individually isolated cells that are positioned to touch each other do not show this charge coupling. Furthermore, collapse of OHC 1 by negative pipette pressure (–0.25 to –0.5 kPa), which abolishes the cell's normal mechanical activity[13], eliminates gating currents in adjacent OHCs (Fig. 1b).

As in OHC 1, the magnitude of the gating currents in OHC 2 reflects the rate of charge redistribution; in this case, however, the rate mirrors that of the deformation of OHC 2. This is indicated by the significant correlation between the OHC 1 clamp time constant (which controls the rate of the OHC mechanical response under whole-cell voltage clamp[6]) and gating current magnitude in OHC 2 ($r^2 = 0.63$; $n = 21$). This is expected, because the OHC gating-current magnitude resulting from stretch is related to the velocity of stretch[15]. The charge redistribution in OHC 2 generates a voltage with a time course that depends on the cells' membrane time constant ($\tau_m = R_m \times C_m$). We looked at this induced voltage under current clamp. In seven cells, the average time constant of voltage decay induced by the impulsive gating current was 8.8 ms. The average membrane resistance of these cells was 272 ± 28 MΩ (mean ± s.e.), the membrane capacitance (at the holding potential) was 35.1 ± 2.02 pF and, consequently, $\tau_m = 9.5$ ms. The initial voltage magnitudes were up to 1.2 mV. The polarity of the induced voltage was negative, corresponding to the movement of positive charge to the outside of the cell membrane. The polarity of the voltage change in mechanically coupled cells is opposite to that of the electrically stimulated cell. Direct currents (d.c.) were not observed in adjacent OHCs, confirming the absence of gap-junction-mediated electrical coupling.

Additional evidence indicates that the transient currents and voltages in adjacent OHCs result from mechanical coupling between OHCs, and that these electrical responses are generated by the displacement of motility/voltage sensors. Figure 2 shows that salicylate, a known blocker of OHC gating currents and motility[20,21], abolishes the gating currents in adjacent OHCs. In our experiments, salicylate probably has two effects: it blocks both the mechanical response of the stimulated cell and the charge movement in the

© 1999 Macmillan Magazines Ltd

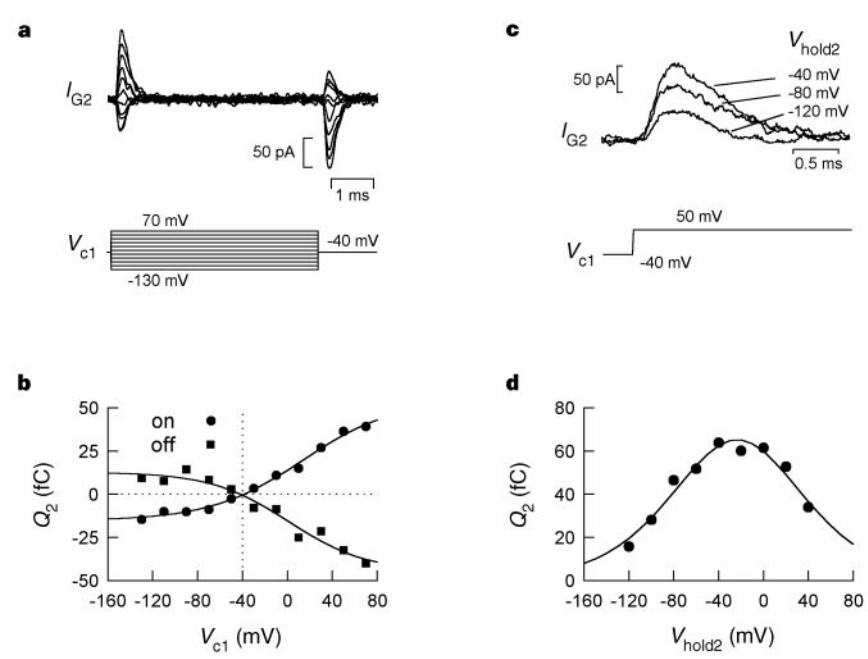

Figure 3 Gating currents are a function of both OHCs' holding potential. **a**, Both OHCs were voltage clamped to –40 mV, and OHC 1 was stepped for 5 ms from –130 to 70 mV (V_{c1}) in 20 mV steps. Gating currents (I_{G2}) in an adjacent OHC are shown in the top trace. The polarity of the currents depends on that of the stimulus voltage in OHC 1. **b**, the *Q*–*V* plot (on and off charge in OHC 2 versus voltage of OHC 1) shows a reversal of gating charge sign at the OHC 1 holding potential. The nonlinearity of the response partially reflects the nonlinear nature of the motility function. **c**, The magnitude of gating current (I_{G2}, top traces) in OHC 2 induced by a fixed voltage step in OHC 1 depends on the membrane (holding) potential of OHC 2. **d**, The *Q*–*V* plot (on charge in OHC 2 versus holding voltage of OHC 2) shows that charge magnitude is a bell-shaped function of OHC 2 holding potential. The data were fit (solid line) to equation (2) with Q_{max} (prior determination from Q_2–V_{c2} function) fixed at 2.99 pC. $\delta V_h = 2.5$ mV; $V_h = -23.5$ mV; $z = 0.65$.

adjacent cell. Further evidence derives from the polarity of the gating currents in adjacent cells (Fig. 3a, b). As expected for a process dependent on the stimulated OHC's mechanical response, the gating current polarity of the adjacent cell reverses at the holding potential of the stimulated cell; depolarization from this potential causes contraction of the cell, whereas hyperpolarization produces elongation. The deformation of adjacent cells will alter the tension on their lateral membranes. Reduced tension effectively shifts the voltage dependence of the *Q*–*V* function in the negative direction, and will evoke a positive gating current[16]. This agrees with the effects measured in adjacent OHCs. The magnitude of charge movement induced by this shift depends on the adjacent cell's membrane (holding) potential and is given by the difference between the two shifted Boltzmann functions[15]:

$$Q(V) = -Q_{max}\delta V_h \frac{ze}{kT}\frac{b}{(1+b)^2} \qquad (2)$$

where δV_h is the magnitude of the V_h shift induced by a change in membrane tension, and b is as in equation (1).

Indeed, this behaviour is seen in our experiments (Fig. 3c, d). The magnitude of gating charge in the adjacent OHC depends on its holding potential, and the bell-shaped function of equation (2) satisfactorily describes the relationship. As the *Q*–*V* function mirrors the OHC's motility function[16], the mechanical activity of coupled OHCs will be affected similarly.

Our data show that, as a result of OHC mechanical activity, lateral interactions exist within the organ of Corti that may significantly affect its responsiveness to sound. We have explored some of the consequences of these interactions. When two pure-tone frequencies are presented to a subject, auditory illusions of additional tonal frequencies and measurable physiological counterparts result[22,23]. Additionally, one tone can be suppressed by another. This distortion arises from nonlinearities in the peripheral auditory system, and in the mammal it results from OHC activity[24,25]. Even within single isolated hair cells, distortion evoked by two-frequency stimulation can be generated by nonlinearities of the sterociliar transducer or by OHC motility[26–28]. We tested whether this type of distortion can arise from interactions between OHCs by simultaneously and independently stimulating each cell of coupled pairs with differing voltage frequencies (OHC 1, $f_1 = 813.8$ Hz; OHC 2, $f_2 = 976.5$ Hz) and observing nonlinear interactions. Under these stimulation conditions, both frequencies are present in the current responses of each cell (Fig. 4). The magnitude of the mechanically induced frequency component (for example, f_2 in OHC 1) is a bell-shaped function of holding potential, indicating, as above, that this component is generated by frequency-following shifts in the voltage dependence of the *Q*–*V* function of the cell. Furthermore, this mechanically generated frequency component suppresses the voltage-evoked frequency component by up to 10%. Finally, the interaction of the two frequency components gives rise to nonlinear intermodulation distortion in each cell (Fig. 4b). The sum and difference distortion components ($f_2 + f_1, f_2 - f_1$) can be observed as little as 20 dB below the mechanically induced primary.

Our data show that nonlinear mechanical interactions occur among OHCs within Corti's organ, and that these interactions generate distortion and suppression that are similar to those found in the intact organ. The generated distortion, seen only in coupled OHCs, may arise not only from the interaction of intrinsic cellular nonlinearities[27,28], but also from nonlinearity in the visco-elastic coupling between cells. The mechanical coupling strength, based on ratios of charge or current, is up to 10%. However, the degree of mechano-electrical coupling among OHCs may be greater *in vivo* than is demonstrated here, as physical coupling in our preparations was probably compromised by the isolation procedure.

It is believed that passive basilar-membrane tuning is enhanced by feedback from OHC mechanical activity[3]; however, based solely on mechanical activity evoked by passive tuning, sharpening would not be expected. The consequence of OHC coupling is twofold for adjacent cells; the voltage dependence of motility is altered, and a voltage of opposite phase is evoked. These mechanically generated

© 1999 Macmillan Magazines Ltd

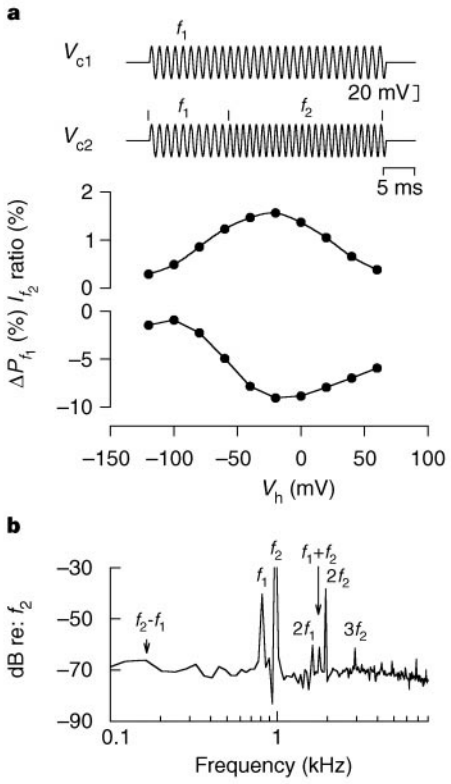

Figure 4 Both OHCs were voltage clamped to –40 mV and independently stimulated with pure sine-wave voltages. **a**, The upper two traces show the voltage stimuli delivered independently to each cell. During the initial part of the stimulus duration, each cell received a 20 mV peak sine wave at $f_1 = 813.8$ Hz; in the latter three-quarters of the stimulus duration, the OHC 2 frequency was switched to 976.5 Hz. Fast Fourier transform analysis was limited to the last half of stimulus duration to avoid transient responses. Comparisons were made before and after uncoupling by collapsing OHC 2. The upper plot shows the ratio of mechanically induced f_2 current (I_{f2}) in OHC 1 due to f_2 voltage stimulation in OHC 2. The ratio of the power of the f_1 component in the response of OHC 1 before and after OHC 2 was collapsed was also obtained. The change in this ratio (ΔP_{f1}) is shown in the lower plot. Negative percentage means that the f_1 response after collapse of OHC 2 was larger than that before; in other words, the mechanically induced f_2 component in OHC 1 suppressed the f_1 response in OHC 1. **b**, The spectrum of current response in OHC 2. The magnitude (in dB) is referenced to f_2 magnitude. Besides harmonic distortion products, the peak of sum frequency distortion ($f_1 + f_2$) is clearly visible.

lateral interactions may allow basilar membrane motion to be selectively enhanced at a particular location where passive vibration is maximal. In nonlinear systems, 10% feedback can have enormous consequences. The likely increase in OHC coupling with increasing frequency, supported by morphological evidence[17], may explain the finding that tuning is sharper at higher characteristic frequencies. In this model, distortion in the cochlea arises from the very process that promotes greater frequency resolution. □

Methods

Pieces of the organ of Corti, containing between 3 and more than 50 OHCs with associated Deiters' cells, were freshly isolated from the guinea-pig cochlea, and adjacent OHCs were separately whole-cell voltage clamped at room temperature using an Axon 200A and 200B amplifier. Membrane voltages were corrected for the effects of residual series resistance, which ranged from 3 to 7 MΩ. We used ionic blocking solutions to remove voltage-dependent ionic conductances so that capacitive currents could be analysed in isolation[29]. Gating currents were extracted using the P/-4 technique[30]. Pipette crosstalk artefacts at the onset of traces (first 50 μs) were subtracted from the data, using the artefacts obtained in the absence of mechanical coupling. All data collection and most analyses were performed with an in-house-developed, Windows-based whole-cell voltage-clamp program, jClamp (www.med.yale.edu/surgery/otolar/santos/jclamp.html), using a Digidata 1200 board (Axon).

Received 29 January; accepted 1 April 1999.

1. von Békésy, G. *Experiments in Hearing* (McGraw-Hill, New York, 1960).
2. Narayan, S. S., Temchin, A. N., Recio, A. & Ruggero, M. A. Frequency tuning of basilar membrane and auditory nerve fibers in the same cochleae. *Science* **282,** 1882–1884 (1998).
3. Dallos, P. The active cochlea. *J. Neurosci.* **12,** 4575–4585 (1992).
4. Brownell, W. E., Bader, C. R., Bertrand, D. & de Ribaupierre, Y. Evoked mechanical responses of isolated cochlear outer hair cells. *Science* **227,** 194–196 (1985).
5. Santos-Sacchi, J. & Dilger, J. P. Whole cell currents and mechanical responses of isolated outer hair cells. *Hear. Res.* **35,** 143–150 (1988).
6. Santos-Sacchi, J. On the frequency limit and phase of outer hair cell motility: effects of the membrane filter. *J. Neurosci.* **12,** 1906–1916 (1992).
7. Dallos, P. & Evans, B. N. High frequency motility of outer hair cells and the cochlear amplifier. *Science* **267,** 2006–2009 (1995).
8. Gale, J. E. & Ashmore, J. F. An intrinsic frequency limit to the cochlea amplifier. *Nature* **389,** 63–66 (1997).
9. Xue, S., Mountain, D. C. & Hubbard, A. E. Electrically evoked basilar membrane motion. *J. Acoust. Soc. Am.* **97,** 3030–3041 (1995).
10. Nuttall, A. L. & Ren, T. Electromotile hearing: evidence from basilar membrane motion and otoacoustic emissions. *Hear. Res.* **92,** 170–177 (1995).
11. Mammano, F. & Ashmore, J. F. Reverse transduction measured in the isolated cochlea by laser Michelson interferometry. *Nature* **365,** 838–841 (1993).
12. Ashmore, J. F. Forward and reverse transduction in the mammalian cochlea. *Neurosci. Res. (suppl.)* **12,** 39–50 (1990).
13. Santos-Sacchi, J. Reversible inhibition of voltage dependent outer hair cell motility and capacitance. *J. Neurosci.* **11,** 3096–3110 (1991).
14. Iwasa, K. H. Effect of stress on the membrane capacitance of the auditory outer hair cell. *Biophys. J.* **65,** 492–498 (1993).
15. Gale, J. E. & Ashmore, J. F. Charge displacement induced by rapid stretch in the basolateral membrane of the guinea-pig outer hair cell. *Proc. R. Soc. Lond. B* **255,** 243–249 (1994).
16. Kakehata, S. & Santos-Sacchi, J. Membrane tension directly shifts voltage dependence of outer hair cell motility and associated gating charge. *Biophys. J.* **68,** 2190–2197 (1995).
17. Vater, M., Lenoir, M. & Pujol, R. Ultrastructure of the horseshoe bat's organ of Corti. II. Transmission electron microscopy. *J. Comp. Neurol.* **318,** 380–391 (1992).
18. Huang, G.-J. & Santos-Sacchi, J. Mapping the distribution of the outer hair cell motility voltage sensor by electrical amputation. *Biophys. J.* **65,** 2228–2236 (1993).
19. Huang, G.-J. & Santos-Sacchi, J. Motility voltage sensor of the outer hair cell resides within the lateral plasma membrane. *Proc. Natl Acad. Sci. USA* **91,** 12268–12272 (1994).
20. Tunstall, M. J., Gale, J. E. & Ashmore, J. F. Action of salicylate on membrane capacitance of outer hair cells from the guinea-pig cochlea. *J. Physiol. (Lond.)* **485,** 739–752 (1995).
21. Kakehata, S. & Santos-Sacchi, J. Effects of lanthanides and salicylate on outer hair cell motility and associated gating charge. *J. Acoust. Soc. Am.* **41,** 676–689 (1967).
22. Goldstein, J. L. Auditory nonlinearity. *J. Acoust. Soc. Am.* **41,** 676–689 (1967).
23. Goldstein, J. L. & Kiang, N. Y. S. Neural correlates of the aural combination tone 2f1-f2. *Proc. IEEE* **56,** 981–992 (1968).
24. Dallos, P. & Harris, D. in *Psychophysics and Physiology of Hearing* (eds Evans, E. F. & Wilson, J. P.) 147 (Academic, London, 1977).
25. Dallos, P., Harris, D. M., Relkin, E. & Cheatham, M. A. in *Psychophysical Physiological and Behavioural Studies in Hearing* (eds van den Brink, G. & Bilsen, F. A.) 242–249 (Delft Univ. Press, Holland, 1980).
26. Jaramillo, F., Markin, V. S. & Hudspeth, A. J. Auditory illusions and the single hair cell. *Nature* **364,** 527–529 (1993).
27. Takahashi, S. & Santos-Sacchi, J. Distortion component analysis of outer hair cell motility-related gating charge. *J. Membr. Biol.* (in the press).
28. Santos-Sacchi, J. Harmonics of outer hair cell motility. *Biophys. J.* **65,** 2217–2227 (1993).
29. Santos-Sacchi, J., Kakehata, S. & Takahashi, S. The outer hair cell membrane potential directly affects the voltage dependence of motility-related gating charge. *J. Physiol. (Lond.)* **510,** 225–235 (1998).
30. Bezanilla, F. & Armstrong, C. M. Inactivation of the sodium channel. I. Sodium current experiments. *J. Gen. Physiol.* **70,** 549–566 (1977).

Acknowledgements. We thank M. Mazzucco for technical help. This work was supported by a grant from NINCDS to J.S.S.

Correspondence and requests for materials should be addressed to J.S.S. (e-mail: joseph.santos-sacchi@yale.edu).

Signals from the reproductive system regulate the lifespan of *C. elegans*

Honor Hsin & Cynthia Kenyon

Department of Biochemistry and Biophysics, University of California at San Francisco, San Francisco, California 94143-0448, USA

Understanding how the ageing process is regulated is a fascinating and fundamental problem in biology. Here we demonstrate that signals from the reproductive system influence the lifespan of the nematode *Caenorhabditis elegans*. If the cells that give rise to the germ line are killed with a laser microbeam, the lifespan of the

© 1999 Macmillan Magazines Ltd